

Holographic Dual to Conical Defects: II. Colliding Ultrarelativistic Particles

D.S. Ageev^a I.Ya. Aref'eva^a

^a*Steklov Mathematical Institute, Russian Academy of Sciences, Gubkin str. 8, 119991
Moscow, Russia*

E-mail: ageev@mi.ras.ru, arefeva@mi.ras.ru

ABSTRACT: We study instant conformal symmetry breaking as a holographic effect of ultrarelativistic particles moving in the AdS_3 spacetime. We give the qualitative picture of this effect probing it by two-point correlation functions and the entanglement entropy of the corresponding boundary theory. We show that within geodesic approximation the ultra-relativistic massless defect due to gravitational lensing of the geodesics, produces a zone structure for correlators with broken conformal invariance. Meanwhile, the holographic entanglement entropy also exhibits a transition to the non-conformal behaviour. Two colliding massless defects produce more diverse zone structure for correlators and the entanglement entropy.

KEYWORDS: AdS/CFT correspondence, holography, conical defects, thermalization, holographic entanglement entropy

Contents

1	Introduction	1
2	Setup	2
3	Correlators on the boundary of AdS_3 deformed by moving defects in the bulk	5
3.1	One ultra-relativistic defect	5
3.2	Two colliding ultra relativistic particles.	9
4	Holographic Entanglement Entropy Calculation	11
4.1	One massless defect.	11
4.2	Two colliding particles	12
5	Conclusion	16

1 Introduction

In this paper we continue to study two-dimensional quantum field theory on the boundary of the AdS_3 space deformed by point particles moving in the bulk within the AdS/CFT correspondence. In the previous paper [1] we have studied deformations by massive moving particles in AdS_3 . Similar problems have been investigated in the early papers [2–5] for various models. For motivation to study these problems see [1] and references therein.

In papers [2–5], [1] the group theoretical language is used to describe the conical defects [6–8] by the corresponding cutting and gluing procedure. To calculate the two-point boundary correlators we use the geodesic approximation proposed in this context in [2]. The ultrarelativistic point particle, starting from the boundary of the cylinder shrinks the bulk along the worldline symmetrically with respect to the starting point [8]. As the particle penetrates the bulk of AdS_3 deeper geodesics connecting the boundary points exhibit lensing effects. A similar effect takes place for massive particles [2–5], [1] and due to this effect one gets the zone structure for two-point correlators of the boundary theory. Considering collisions of two ultrarelativistic particles we get even more complicated structure for geodesics, that lead to a multi-zone structure for two-point correlators. Namely, around the edges of the shrinking space we get the focusing of geodesics due to winding on the wedges of the defect in a rather nontrivial way. Near the endpoints the winding geodesics dominate, while away from the location of wedges, dominate the non-winding ones. There

is also an intermediate zone, where both families of geodesics contribute, creating some kind of resonance. There are also discontinuities separating different zones, they are localized and propagate on the boundary of AdS_3 with the constant speed.

The study of the holographic entanglement entropy (HEE) [9] becomes a rapidly developing subject with a broad range of applications due relative simplicity of entanglement entropy realization in holography and wide variety of modifications of basic examples [10–15]. In this paper we calculate the HEE for 2-dimensional theories on the circle with varying radius. As holographical gravity models we consider the same models as in the first part of the paper, the AdS_3 spacetime deformed by one or two ultrarelativistic particles.

The paper is organized as follows. In Section 2 we review the AdS_3/CFT_2 setup with colliding point particles in the bulk. In Section 3 we compute the two-point correlation function using the geodesic approximation and present the results of the calculations. In Section 4 we compute the holographic entanglement entropy in presence of ultra relativistic particles. In the conclusion we summarize the obtained results and discuss future perspectives related with investigations of collisions of two ultrarelativistic particles.

2 Setup

Let us briefly recall the group structure of the description of ultrarelativistic particle deformation of the AdS_3 space on group theoretical language [6–8].

Points of AdS_3 can be represented as $SL(2)$ group elements of real 2×2 matrices

$$\mathbf{x} = x_3 \mathbf{1} + \sum_{\mu=0,1,2} \gamma_\mu x^\mu = \cosh \chi \mathbf{\Omega}(t) + \sinh \chi \mathbf{\Gamma}(\phi), \quad (2.1)$$

where

$$\mathbf{1} = \begin{pmatrix} 1 & 0 \\ 0 & 1 \end{pmatrix}; \quad \gamma_0 = \begin{pmatrix} 0 & 1 \\ -1 & 0 \end{pmatrix}; \quad \gamma_1 = \begin{pmatrix} 0 & 1 \\ 1 & 0 \end{pmatrix}; \quad \gamma_2 = \begin{pmatrix} 1 & 0 \\ 0 & -1 \end{pmatrix}, \quad (2.2)$$

and

$$\mathbf{\Omega}(t) = \cos t \mathbf{1} + \sin t \gamma_0 \quad \mathbf{\Gamma}(\phi) = \cos \phi \gamma_1 + \sin \phi \gamma_2, \quad (2.3)$$

where (t, χ, ϕ) are "barrel" coordinates, here we assume, that $\chi \geq 0$, $\phi \simeq \phi + 2\pi$, $-\pi/2 < t < \pi/2$.

We will also use the Poincare disk coordinate r , related with χ via

$$r = \tanh\left(\frac{\chi}{2}\right). \quad (2.4)$$

In the Poincare disc coordinates the AdS_3 metric is:

$$ds^2 = - \left(\frac{1+r^2}{1-r^2} \right)^2 dt^2 + \left(\frac{2}{1-r^2} \right)^2 (dr^2 + r^2 d\phi^2), \quad (2.5)$$

where $r < 1$.

Let us consider a massless particle with a lightlike momentum vector pointing along the x -direction. Its holonomy is:

$$u = 1 + \tan \epsilon \begin{pmatrix} 0 & 2 \\ 0 & 0 \end{pmatrix}, \quad u^{-1} = 1 - \tan \epsilon \begin{pmatrix} 0 & 2 \\ 0 & 0 \end{pmatrix}. \quad (2.6)$$

The isometry transformation related to the holonomy has the form

$$\mathbf{x} \rightarrow \mathbf{x}^* = u^{-1} \mathbf{x} u. \quad (2.7)$$

Lightlike particle worldline is the set of fixed points of this isometry, with $r = \tan(t/2)$ and $\phi = 0$. To construct the region that the particle cuts out from AdS space, one proceeds as following [8]. First, we switch to the ADM-like point of view, so that AdS can be considered as a Poincaré disc evolving in time. Then, one looks for a pair of some special curves w_{\pm} on the constant time sections. These curves are mapped onto each other by the given isometry. Finally, we cut out the wedge between these curves, and identify the faces according to the isometry.

Note, that it takes only a finite amount of time for the particle to travel through the whole space. The particle start position is at $t = -\pi/2$, and the final position is at $t = \pi/2$. We consider deformation only for this time interval $-\pi/2 < t < \pi/2$ and we expect the space manifold to be a Poincaré disc with a wedge cut out.

A point $(t, r, -\phi) \in w_-$ is mapped onto $(t, r, \phi) \in w_+$ under the isometry action. The matrices representing these points are

$$\mathbf{w}_{\pm} = \frac{1+r^2}{1-r^2} \mathbf{\Omega}(t) + \frac{2r}{1-r^2} \mathbf{\Gamma}(\pm\phi). \quad (2.8)$$

Writing the relation

$$\mathbf{u} \mathbf{w}_+ = \mathbf{w}_- \mathbf{u} \quad (2.9)$$

one finds [8], that the faces w_+ and w_- are uniquely determined by the following equations

$$w_{\pm} : \frac{2r}{1+r^2} \sin(\epsilon \pm \phi) = \sin t \sin \epsilon. \quad (2.10)$$

The curves w_+ and w_- intersect at the the fixed point of the isometry, lightlike worldline

$$r = \tan(t/2). \quad (2.11)$$

The spacetime manifold is obtained by cutting out the wedge behind the particle and identifying the faces of the wedge defined by equations (2.10). The resulting spacetime manifold has constant curvature everywhere, excepting the world line.

In Fig.1 these curves are shown for different constant time sections. In Fig.2 the wedge to be removed is shown.

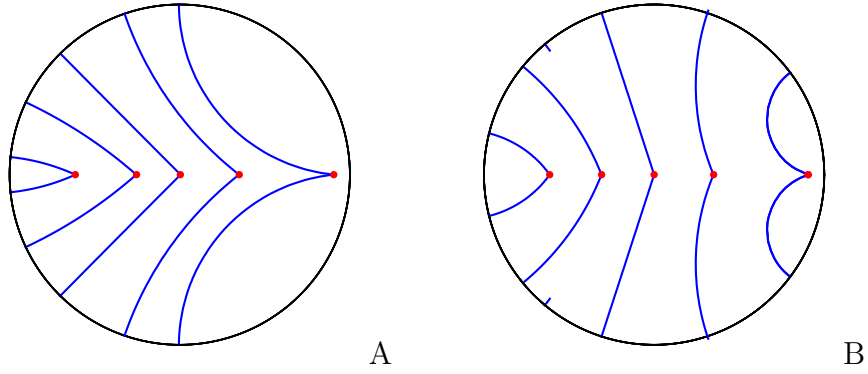


Figure 1. The plot of the wedges w_{\pm} , $\epsilon = \pi/4$ (A) and $\epsilon = 0.45\pi$ (B), for different constant time sections. From the left to right (on each plot) curves correspond to constant time t sections for $t = -1.1, -0.4, 0, 0.3, 1.47$.

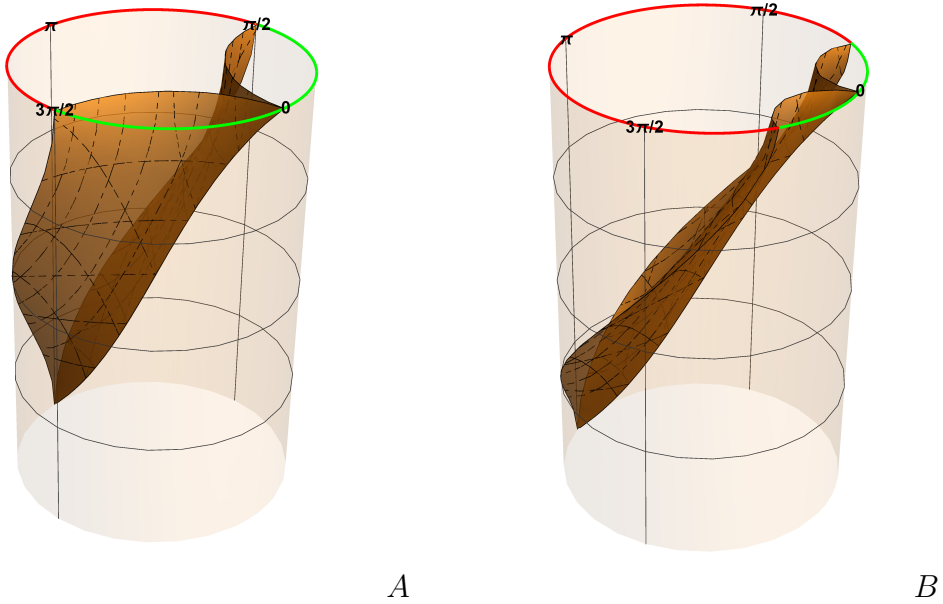


Figure 2. The plot of wedge faces that the point particle produces. The green line on the boundary shows the allowed zone for the final time moment, $t = \pi/2$, the red coloring corresponds to the cut out space. Here we take $\epsilon = \pi/4$ (A) and $\epsilon = 0.45\pi$ (B).

In [8] the AdS_3 space deformed by two ultrarelativistic particles starting from the opposite points of the AdS_3 boundary has been also considered.

As it was mentioned, point sources deform AdS_3 in a local way, so for each particle and wedge faces we can take the result just mentioned above. In Fig.3. A we plot the process of collision for two ultrarelativistic particles starting with angles $\phi = 0$ and $\phi = \pi$ at the moment $t = -\pi/2$, i.e. before $t = 0$. The space between

faces of the wedges on the left and on the right side are deleted. The picture after collision is presented in Fig.3.B.

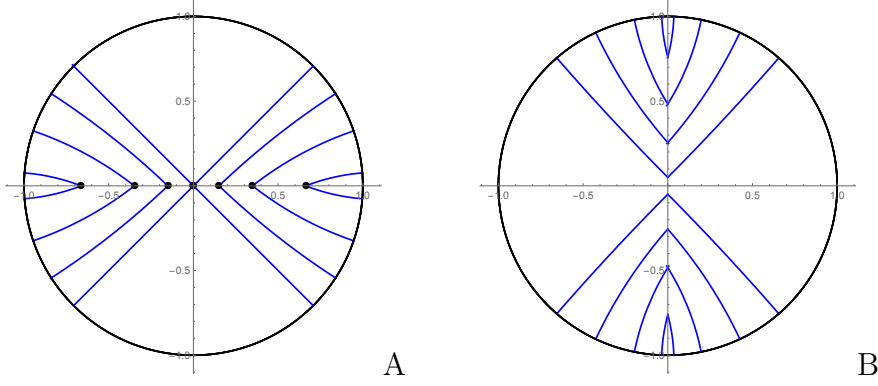


Figure 3. The plot of two colliding massless particles picture for $\epsilon = \pi/4$, before collision (A) and after collision (B) for different times t . On the left plot $t = -1.17, -0.67, -0.3, 0..$ In the right plot $t = 0.1, 0.5, 0.9, 1.3$.

3 Correlators on the boundary of AdS_3 deformed by moving defects in the bulk

3.1 One ultra-relativistic defect

Let us consider the two-point correlator on the boundary of AdS_3 deformed by one massless particle¹

The two-point correlator on the boundary of AdS_3 deformed by one massless particle is:

$$G_{\epsilon,\Delta}(\phi_a, t_a, \phi_b, t_b) = \left(\frac{1}{2 |\cos(t_a - t_b) - \cos(\phi_a - \phi_b)|} \right)^\Delta \Theta_{ncr}(t_a, \phi_a; t_b, \phi_b; \epsilon) \quad (3.1)$$

$$+ \left(\frac{1}{2 |\cos(t_{a\#} - t_b) - \cos(\phi_{a\#} - \phi_b)|} C_{a\#}^{-1/2} \right)^\Delta \Theta_{cr}(t_{a\#}, \phi_{a\#}; t_b, \phi_b; \epsilon).$$

where

$$C_{b^*} = ((2 \tan^2(\epsilon) + 1) \sin(t_b) - 2 \tan(\epsilon) \sec(\epsilon) \sin(\epsilon - \phi_b))^2 + \cos^2(t_b) \quad (3.2)$$

$$C_{b\#} = ((2 \tan^2(\epsilon) + 1) \sin(t_b) - 2 \tan(\epsilon) \sec(\epsilon) \sin(\epsilon + \phi_b))^2 + \cos^2(t_b) \quad (3.3)$$

¹Here we mean a deformation of the universal two-point correlator, given by eq.(2.76) in [1]. It is related with the Wightman, retarded and causal correlators by well-known formulae, see Sec.2.3.4. in [1].

are the renormalization factors (see [1] for more details). The function Θ_{ncr} is defined as follows:

- $\Theta_{ncr}(t_a, \phi_a; t_b, \phi_b; \epsilon) = 1$ if geodesic connecting points (ϕ_a, t_a) and (ϕ_b, t_b) does not cross the wedge at some time;
- $\Theta_{ncr}(t_a, \phi_a; t_b, \phi_b; \epsilon) = 0$ if geodesic connecting points (ϕ_a, t_a) and (ϕ_b, t_b) crosses the wedge at some time.

Θ_{cr} is defined as follows:

- $\Theta_{cr}(t_a, \phi_a; t_b, \phi_b) = 1$ if geodesic crosses the nearest from the point b face of the wedge at any time;
- $\Theta_{cr}(t_a, \phi_a; t_b, \phi_b) = 0$ if geodesic does not cross the nearest face of the wedge from the point b .

Calculating supports of functions Θ_{cr} and Θ_{ncr} numerically we find which geodesics contribute to the correlator. Generally speaking, there are three different possibilities for geodesic configurations connecting two points on the boundary:

- there is a geodesic connecting a and b that does not cross the wedges (we call this geodesic the basic, or the non-winding one) and there is no winding geodesic connecting a and b (i.e. there is no geodesic connecting a and b and crossing the wedge)
- there is a winding geodesic connecting a and b and there is no one geodesic connecting a and b
- there is a basic geodesic connecting a and b and simultaneously there is a winding geodesic connecting a and b .

In Fig.4 and Fig.5 we plot the different cases of geodesic configurations for different values of the parameter ϵ . If the basic geodesic does not cross the wedge it contributes to the propagator, and conversely, if the geodesics connecting images does not cross the wedge, it does not act as a winding geodesic.

In Fig.4.A the black curve does not intersect the wedges and winding geodesics (green and red lines) intersect the wedges. In this case both contribute in (3.1). In Fig.4.B the black curve is noncrossing and red and green curves do not cross the wedge faces too. In this case only the non-winding geodesic (the black curve) contributes. In Fig.4.C the black curve intersects the wedge, geodesics relating corresponding image points also intersect the wedge, so only the winding geodesic contributes. The same picture takes place for geodesics presented in Fig.5. A, B and C.

Let us see the influence of moving particle on the two-point function $G_{\epsilon, \Delta}(\phi_1, t_1, \phi_2, t_2)$. Let us take one of the points, namely (ϕ_1, t_1) , to be fixed. Suppose, that ϕ_1 and ϕ_2

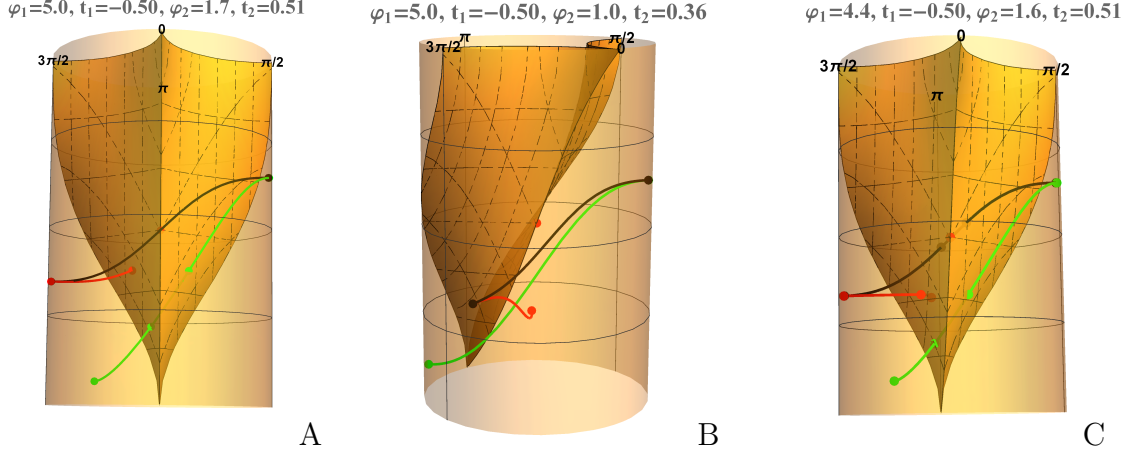


Figure 4. The black curves on plots A, B and C are the basic geodesics, the red and green ones are winding geodesics. Boundary points (ϕ_a, t_a) and (ϕ_b, t_b) correspond to the black geodesic endpoints. $\epsilon = \frac{\pi}{4}$.

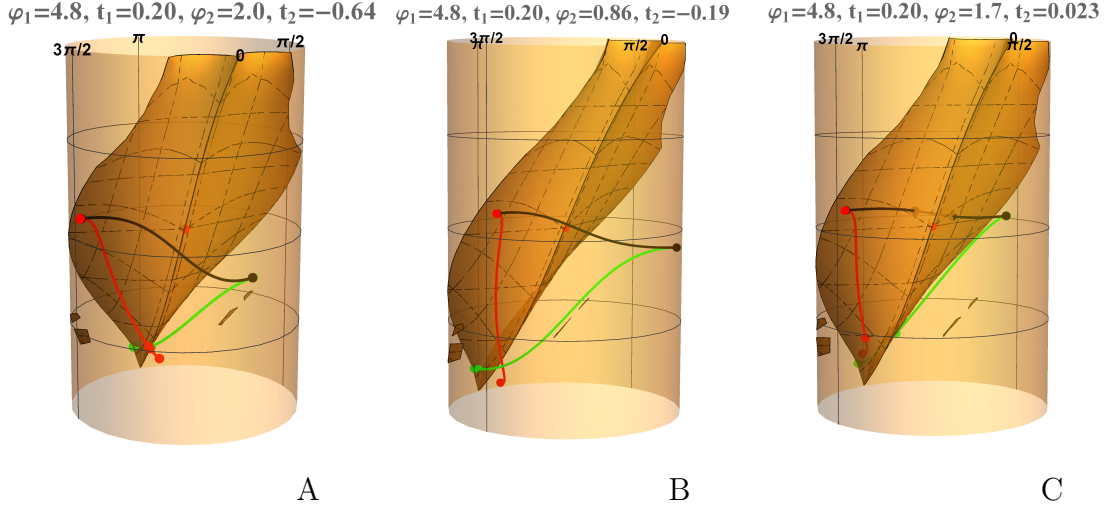


Figure 5. The black curves on plots A, B and C are the basic geodesic, the red and green are winding ones. Boundary points (ϕ_a, t_a) and (ϕ_b, t_b) correspond to the black curve endpoints. $\epsilon = 0.4\pi$.

are located on the opposite halves of the AdS_3 boundary with respect to the lightlike worldline, i.e. $\phi_1 \in (\pi, 2\pi)$, $\phi_2 \in (0, \pi)$, and time $t_1, t_2 \in (-\frac{\pi}{2}, \frac{\pi}{2})$, i.e. we study the quantity:

$$\mathcal{G}_{\epsilon, \Delta, \phi_1, t_1}(\phi, t) = G_{\epsilon, \Delta}^{-1}(\phi_1, t_1, \phi, t). \quad (3.4)$$

In Fig.6 and Fig.7 we plot $\mathcal{G}_{\epsilon,\Delta,\phi_1,t_1}(\phi,t)$ for different ϵ , t_1 and ϕ_1 . From Fig.6 and Fig.7 we see, that near the edge of the living space there is a nontrivial change in the correlator. We call this zone a pulse. Pulse propagates from the edges of the defect and its size is changed with time. In Fig.6.A we can see, that the discontinuity is formed at the moment $t = -\frac{\pi}{2}$, near the point on the boundary, wherefrom the massless particle starts, then this discontinuity propagates with nearly constant speed. On the left side from the discontinuity the correlator is not changed and here the conformal symmetry is not broken. In Fig.6.B we see how additional discontinuity appears, due to mixing of different geodesic contributions and we get a resonance.

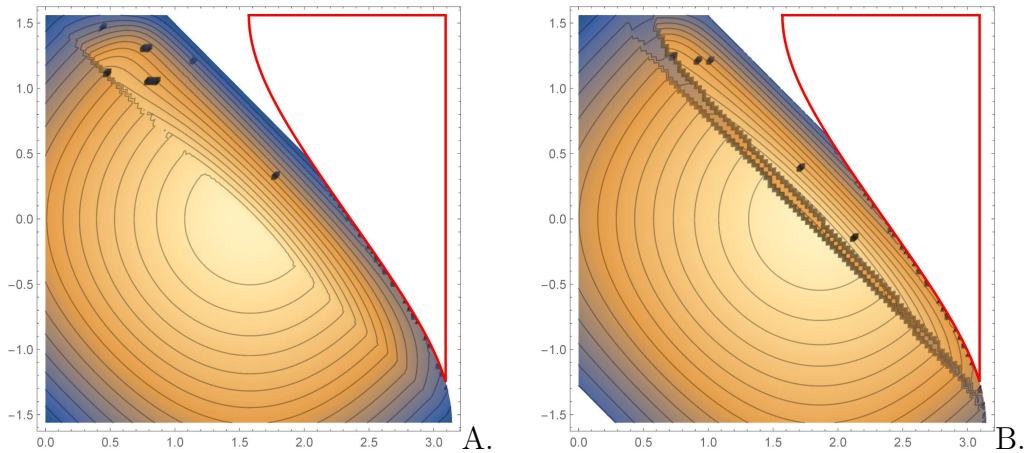


Figure 6. Density plot of the function (3.4). The angular coordinate corresponds to the x-axis and time coordinate to the y-axis. The point particle parameter value $\epsilon = \frac{\pi}{4}$. The red thick curve corresponds to the boundary of the living space. A. Fixed angle $\phi_1 = \frac{3\pi}{2}$ and time $t_1 = 0$, conformal dimension value is $\Delta = 1$. The thick black line near the diagonal corresponds to the discontinuity in the correlator due to the presence of different contributions. B. Fixed angle $\phi_1 = 5$ and time $t_1 = 0$, conformal dimension value is $\Delta = 1$. Two thick black lines near the diagonal correspond to the discontinuity in the correlator due to different contributions presence.

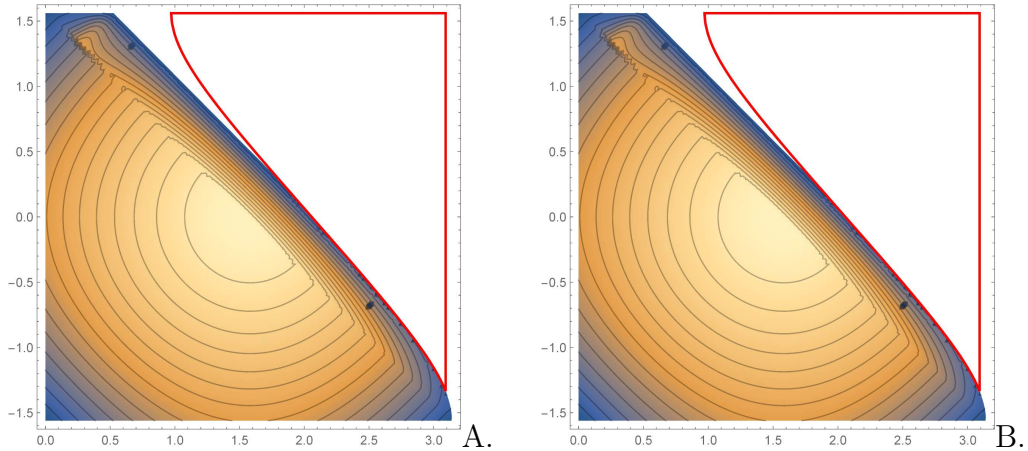


Figure 7. Density plot of the functions (3.4). The point particle parameter value $\epsilon = 1$. The angular coordinate corresponds to the x-axis and time coordinate to the y-axis. The red thick curve corresponds to the boundary of the living space. The conformal dimension is $\Delta = 1$ for both plots A. and B. A. Fixed angle $\phi_1 = \frac{3\pi}{2}$ and time $t_1 = 0$. The thick black line near the diagonal corresponds to the discontinuity in the correlator due to the presence of different contributions. B. Fixed angle $\phi_1 = 5$ and time $t_1 = 0$. Two thick black lines near the diagonal correspond to the discontinuity in the correlator due to different contributions presence

3.2 Two colliding ultra relativistic particles.

Let us consider two colliding point particles in the AdS_3 . It includes more possibilities for geodesics to wind on the faces of the defect and the picture is more involved for this case.

There are two different cases:

- The first one is when we take two points on the opposite sides of cylinder, symmetrically with respect to the line of collision, i.e. we consider correlator $G(\phi_1, t_1, \phi_2, t_2)$, where $\pi < \phi_1 < 2\pi$ and $0 < \phi_2 < \pi$. Time is taken to be $-\pi/2 < t_1, t_2 < \pi/2$. In this case we have the contribution coming from two types of geodesics: the basic geodesic and the geodesics passing once through each defect (see Fig. 8)
- The second one is when we take both points on one side of the boundary, i.e. $\pi < \phi_1 < 2\pi$ and $\pi < \phi_2 < 2\pi$. In this case the two-point correlator obtains two contributions, one from the basic geodesic, and one from the geodesic that winds two times. First it passes through the lower face of the left wedge, then through the upper face of the right wedge. The schematic illustration of this case is presented in Fig. 9A.

In this paper we consider only the first case from the above list. It corresponds to the long-range effects in dual theory. Let us consider the first situation from the above list. The universal correlator for the case when points are on the opposite sides of AdS_3 is:

$$\begin{aligned}
& G(\phi_a, t_a, \phi_b, t_b)_{\epsilon_1, \epsilon_2, \Delta} \tag{3.5} \\
&= \left(\frac{1}{2 |\cos(t_a - t_b) - \cos(\phi_a - \phi_b)|} \right)^\Delta \Theta_{ncr}^{all}(a, b; \epsilon_1) \cdot \Theta_{ncr}^{all}(a, b; \epsilon_2) \\
&+ \left(\frac{1}{2 |\cos(t_{a\#1} - t_b) - \cos(\phi_{a\#1} - \phi_b)|} C_{a\#1}^{-1/2} \right)^\Delta \Theta_{cr}^{ll}(a\#1, b; \epsilon_1) \cdot \Theta_{ncr}^{lu}(a, b\#1; \epsilon_2) \\
&+ \left(\frac{1}{2 |\cos(t_a - t_{b\#2}) - \cos(\phi_a - \phi_{b\#2})|} C_{a\#2}^{-1/2} \right)^\Delta \Theta_{cr}^{rl}(a\#2, b; \epsilon_2) \Theta_{ncr}^{ru}(a, b\#2; \epsilon_1)
\end{aligned}$$

The term in the first line corresponds to the basic geodesic contribution, the second line corresponds to geodesic winding through the left wedge and the third line corresponds to the contribution from the geodesic winding through the right wedge. Here we use different functions Θ defined as following.

Function $\Theta_{ncr}^{all}(a, b; \epsilon) = 1$ if the geodesic connecting two points a and b does not cross any wedge and $\Theta_{ncr}^{all}(a, b; \epsilon) = 0$ otherwise.

Function $\Theta_{cr}^{ll}(a, b; \epsilon) = 1$ if the geodesic crosses left lower face of the wedge and $\Theta_{cr}^{ll}(a, b; \epsilon) = 0$ otherwise.

Function $\Theta_{cr}^{rl}(a, b; \epsilon) = 1$ if the geodesic crosses right lower face of the wedge and $\Theta_{cr}^{rl}(a, b; \epsilon) = 0$ otherwise.

Function $\Theta_{ncr}^{lu}(a, b; \epsilon) = 1$ if the geodesic does not cross left upper face of the wedge and $\Theta_{ncr}^{lu}(a, b; \epsilon) = 0$ otherwise.

Function $\Theta_{ncr}^{ru}(a, b; \epsilon) = 1$ if the geodesic does not cross right upper face of the wedge and $\Theta_{ncr}^{ru}(a, b; \epsilon) = 0$ otherwise.

In Fig.10 and Fig.11 we present the dependence of the inverse correlators on the boundary in the case of two massless particles in the bulk. Here $\phi_1 = 3\pi/2$ and $\phi = 5$. In all these plots we see two pulse zones coming from each boundary. We see asymmetry in the right columns of Fig.10 and Fig.11. Asymmetry is related with the asymmetrical position of the point ϕ_1 with respect to the collision line. In some time these two pulses collide, forming another structure. Note, that the asymmetry is conserved during the collision process.

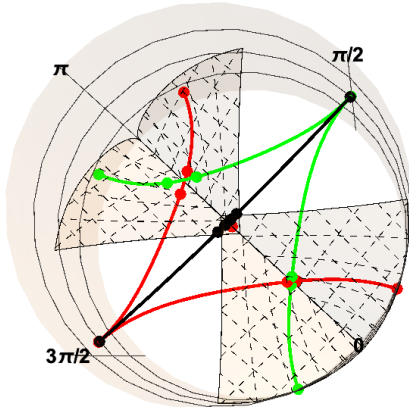


Figure 8. Illustration of multiple geodesics configuration for two certain points (the black curve endpoints) on the boundary. Black curve is the basic geodesic, red geodesics pass through the left and right wedge faces, green geodesics are their image under the isometry action (here we take $\epsilon = \pi/4$ for both defects).

4 Holographic Entanglement Entropy Calculation

4.1 One massless defect.

In this section we calculate the HEE for spacelike intervals for different equal time sections of our background. We fix equal time points on the opposite sides of the boundary of the AdS_3 space with respect to the particle worldline, $t_1 = t_2 = t_0$. To probe the HEE we vary t_0 from $t_0 = -\pi/2$ to $\pi/2$. For a static spacetime the HEE [10] equals² to the minimal renormalized length $L_{ren}(\phi_1, t_0, \phi_2, t_0)$ of the geodesic connecting two points on the boundary, (ϕ_1, t_0) and (ϕ_2, t_0) ,

$$S(\phi_1, \phi_2, t_0) = \min \mathcal{L}_{ren}(\phi_1, t_0, \phi_2, t_0). \quad (4.1)$$

As we can separate the time and space directions in the ADM formalism we can use formula (4.1) in this background. In Fig.12 we plot how the pulse structures described in the previous sections are probed by the HEE. In Fig.12 we plot the dependence of the HEE on t_0 and ϕ_2 for ϕ_1 being fixed and different ϵ . We see that similarly to two-point functions, there exists an expanding pulse-like zone propagating from the point on the boundary where the massless particle has been injected.

²we omit all prefactors in the calculation of the HEE like the gravitational constant etc.

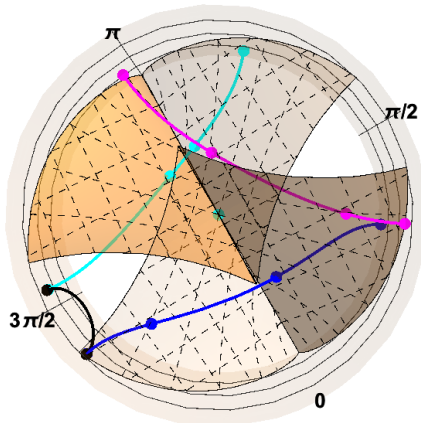


Figure 9. Illustration of one of the additional contributions to the correlator, when points on the boundary (the black curve endpoints) to be taken on one side of the boundary. They wind through both wedges. Black curve is the basic geodesic, the magenta geodesic is an intermediate, and it is the result of application of the isometry induced by left wedge to green geodesic. The blue geodesic is the result of application of the isometry induced by the right wedge to magenta geodesic. Here we take $\epsilon = \pi/4$ for both particles.

From Fig.12.A and Fig.12.B. we see that for some time the HEE remains constant, then it turns to a nonequilibrium regime. For larger intervals this transition to a nonequilibrium regime occurs faster.

4.2 Two colliding particles

In this subsection we probe the HEE evolution in the AdS_3 background deformed by two colliding massless particles.

Again, there are two different cases. The first one is when we probe the HEE evolution for spacelike interval with endpoints placed on the opposite sides of the boundary, with respect to the line of the collision, and the second one is when these points are on the same side with respect to the collision line. The configurations of the geodesics are the same as for calculations two-point correlators, but now we have to take into account only geodesics with minimal renormalized length.

In Fig.13 we plot how the HEE probes the particles collision process, we plot the dependence of HEE on t_0 and ϕ_2 for different ϵ and fixed ϕ_1 . Here red curves correspond to the contracting boundary of the living space. From Fig.13A. we see wide zones, separated by discontinuities coming from each boundary. These zones rapidly grow, and from some moment the regime is changed again in all living space. In Fig.13.B the energy is large, $\epsilon = 0.5$ and in Fig.13.B, $\epsilon = 0.1$ and we see, that

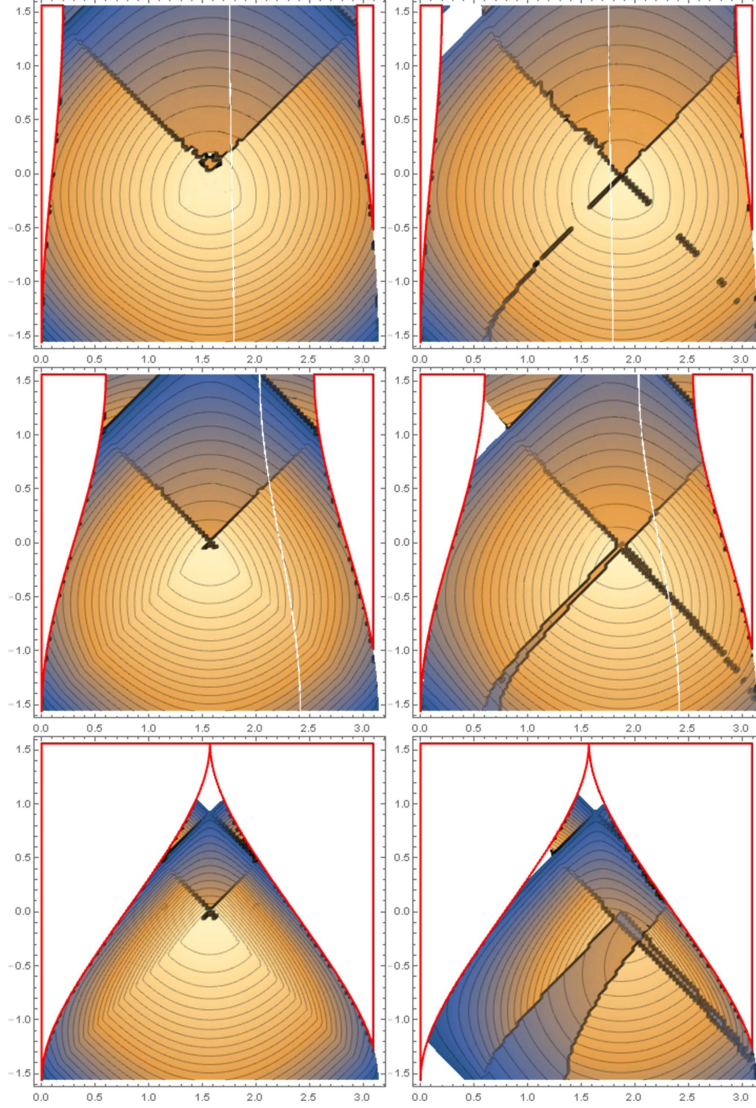


Figure 10. Dependence of the inverse correlators in the case of two massless particles collision. In this case $\phi_1 = \frac{3\pi}{2}$ (left column), $\phi_1 = 5$ (right column) and $t_1 = 0$, conformal dimension $\Delta = 1$ for each plot. Parameters for each plot are $\epsilon = 0.1, 0.3, 0.78$ from top to down. Red curves correspond to boundaries of two dead zones, black curves are boundaries of discontinuities separating pulses.

the size and rapidity of growth for these zones are relatively weak dependent on the value of energy ϵ .

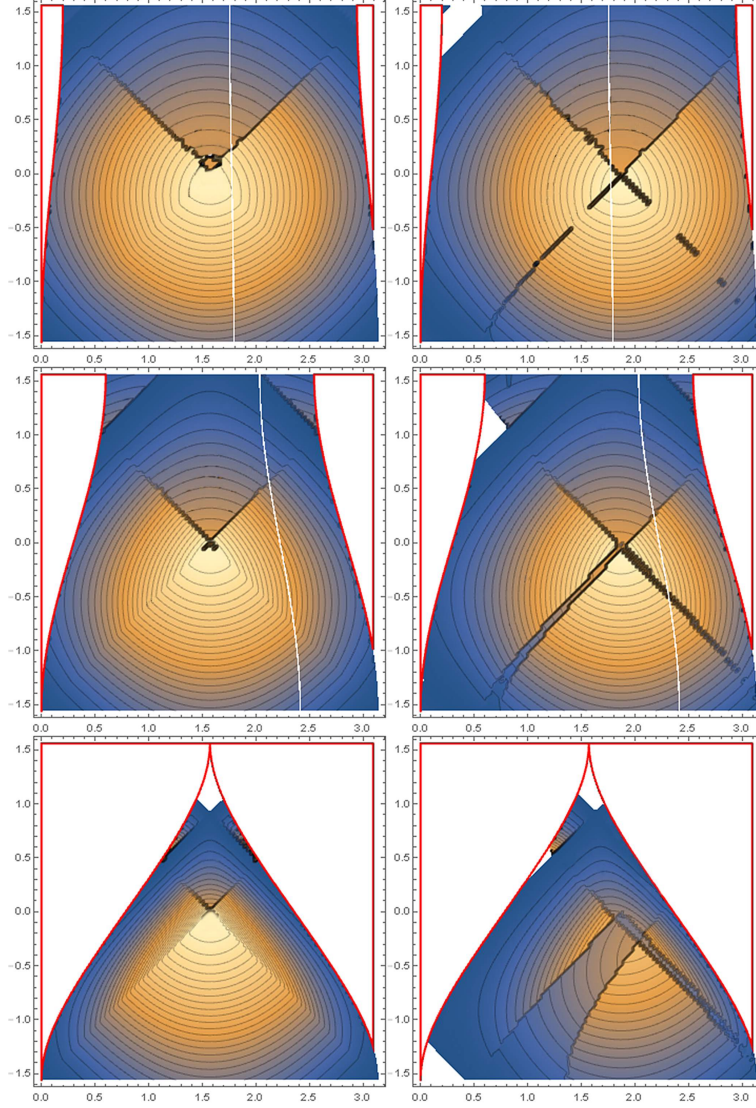


Figure 11. Dependence of the inverse correlators in the case of two massless particles collision. In this case $\phi_1 = \frac{3\pi}{2}$ (left column), $\phi_1 = 5$ (right column) and $t_1 = 0$, conformal dimension $\Delta = 2$ for each plot. Parameters of collision for each plot are $\epsilon = 0.1, 0.3, 0.78$ from top to down. Red curves correspond to boundaries of two dead zones, black curves are boundaries of discontinuities separating pulses

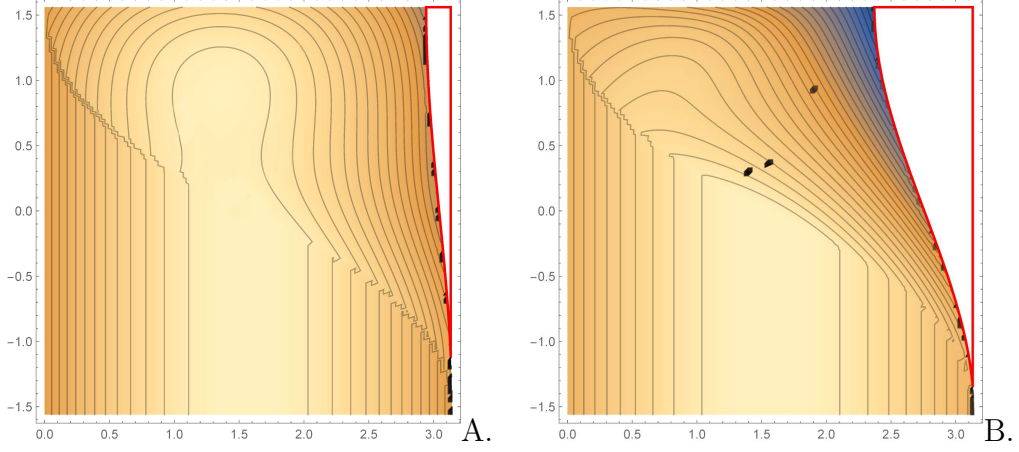


Figure 12. Dependence of the holographic entanglement entropy, calculated with the formula (4.1), on t_0 and ϕ_2 . Here $\phi_1 = \frac{3\pi}{2}$, $\epsilon = 0.78$ (plot A) and $\phi_1 = \frac{3\pi}{2}$, $\epsilon = 0.38$ (plot B). ϕ_2 corresponds to x-axis, t_0 to y-axis.

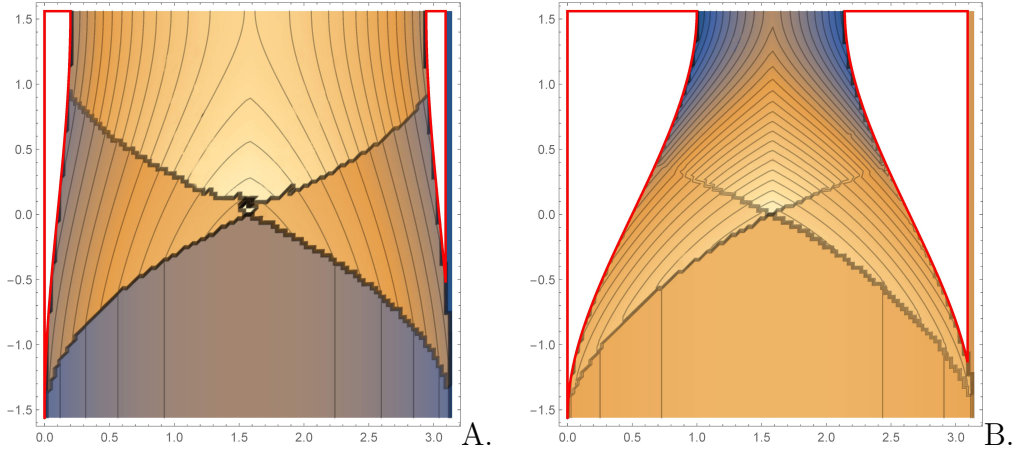


Figure 13. Dependence of the holographic entanglement entropy, calculated with the formula (4.1), on t_0 and ϕ_2 for different ϕ_1 and ϕ_2 . On the plot A. $\epsilon = 0.1$ and $\phi_1 = 3\pi/2$. On plot B. $\epsilon = 0.5$ and $\phi_1 = 3\pi/2$. ϕ_2 corresponds to x-axis, t_0 to y-axis.

5 Conclusion

In this paper we have considered the models of quantum field theory, dual to the AdS_3 space with one ultrarelativistic point-like particle and with two colliding ultrarelativistic point particles. In both cases the dual models live on the spaces with varying sizes. For these models, we have studied two-point correlation functions within the geodesic approximation and the holographic entanglement entropy. From numerical calculations we have seen that these models capture some features of quantum systems under sudden quench and quantum systems with time-dependent volume. We have shown that within geodesic approximation the ultrarelativistic massless defects due to gravitational lensing of the geodesics produce zone structure for correlators. Non-stationary living spaces produce excitation waves, moving along the boundaries from the quench points, i.e. from the points on the boundary where the ultrarelativistic particles is injected. The propagating pulse zone is localized near the ends of the wedge on the boundary. There are also intermediate zones separated by discontinuities which are localized and propagate along the living space with the constant speed. HEE has also nontrivial zone structure. Two colliding massless defects produce more complicated zone structure for correlators and entanglement entropy.

It worth to find out are these discontinuities in the correlator and entropy artifacts of the classical approximation that we used, or they can be seen even in a full solution through the scalar field equation. This question we suppose to investigate in the separated study, that is started in [16].

Acknowledgement

We would like to thank Andrey Bagrov, Mikhail Khramtsov, Maria Tikhanovskaya and Igor Volovich for useful discussions. This work was supported by the Russian Science Foundation (grant No. 14-11-00687).

References

- [1] I.Ya. Aref'eva, D.S.Ageev and M.D. Tikhanovskaya, Holographic Dual to Conical Defects: I. Moving Massive Particle, arXiv:
- [2] V. Balasubramanian and S. F. Ross, "Holographic particle detection," Phys. Rev. D **61**, 044007 (2000) [hep-th/9906226].
- [3] I.Ya. Aref'eva and A. A. Bagrov, Holographic dual of a conical defect, Theoret. and Math. Phys., 182 (2015), 22
- [4] V. Balasubramanian, B. D. Chowdhury, B. Czech and J. de Boer, "Entwinement and the emergence of spacetime," JHEP **1501**, 048 (2015)

- [5] I. Arefeva, A. Bagrov, P. Saterskog and K. Schalm, “Holographic dual of a time machine,” arXiv:1508.04440 [hep-th].
- [6] S. Deser, R. Jackiw, and G. ’t Hooft, *Three dimensional Einstein gravity: dynamics of flat space*, *Ann. Phys.* **152** (1984) 220
- [7] G. ’t Hooft, *Quantization of point particles in (2+1)-dimensional gravity*, *Class. Quantum Grav.* **13** (1996) 1023.
- [8] H. -J. Matschull, “Black hole creation in (2+1)-dimensions,” *Class. Quant. Grav.* **16**, 1069 (1999) [gr-qc/9809087].
- [9] S. Ryu and T. Takayanagi, “Holographic derivation of entanglement entropy from AdS/CFT,” *Phys. Rev. Lett.* **96**, 181602 (2006) [hep-th/0603001].
- [10] T. Nishioka, S. Ryu and T. Takayanagi, “Holographic Entanglement Entropy: An Overview,” *J. Phys. A* **42**, 504008 (2009) [arXiv:0905.0932 [hep-th]].
- [11] M. Nozaki, T. Numasawa and T. Takayanagi, “Holographic Local Quenches and Entanglement Density,” *JHEP* **1305**, 080 (2013) [arXiv:1302.5703 [hep-th]].
- [12] C. T. Asplund, A. Bernamonti, F. Galli and T. Hartman, “Holographic Entanglement Entropy from 2d CFT: Heavy States and Local Quenches,” *JHEP* **1502**, 171 (2015) [arXiv:1410.1392 [hep-th]].
- [13] D. Marolf, H. Maxfield, A. Peach and S. F. Ross, “Hot multiboundary wormholes from bipartite entanglement,” arXiv:1506.04128 [hep-th].
- [14] H. Casini, H. Liu and M. Mezei, “Spread of entanglement and causality,” arXiv:1509.05044 [hep-th].
- [15] T. Hartman and N. Afkhami-Jeddi, “Speed Limits for Entanglement,” arXiv:1512.02695 [hep-th].
- [16] I. Ya. Aref’eva and M. Khramtsov, AdS/CFT prescription for angle-deficit space and winding geodesics, in preparation